crystals

MDPI

Article

Structural Analysis of Coordination Cage/Guest Complexes Prepared with the 'Crystalline Sponge' Methodology

Christopher G. P. Taylor [1], James R. Williams [1], Stephen P. Argent [1,2] and Michael D. Ward [1,*]

[1] Department of Chemistry, University of Warwick, Coventry CV4 7AL, UK
[2] School of Chemistry, University of Nottingham, University Park, Nottingham NG7 2RD, UK
* Correspondence: m.d.ward@warwick.ac.uk

Abstract: The crystalline sponge method has proven invaluable in the preparation and analysis of supramolecular host/guest complexes if the host can be obtained in a suitable crystalline form, allowing the analysis of guest binding modes inside host cavities which can inform other studies into processes such as catalysis. Here, we report the structures of a set of ten host/guest complexes using an octanuclear coordination cage host with a range of small-molecule neutral organic guests including four aromatic aldehydes and ketones, three cyclic lactams, and three epoxides. In all cases, the cavity-bound guests are anchored by a collection of CH•••O hydrogen-bonding interactions between an O atom on the guest and a convergent set of CH protons at a pocket on the cage interior surface. Depending on guest size and the presence of solvent molecules as additional guests, there may be one or two cavity-bound guests, with small aromatic guests forming π-stacked pairs. Some guests (the lactams) participate in additional NH•••F H-bonding interactions with surface-bound fluoroborate anions, which indicate the type of anion/guest interactions thought to be responsible for solution-phase catalytic reactions of bound guests.

Keywords: supramolecular chemistry; host/guest complexes; coordination cages

Citation: Taylor, C.G.P.; Williams, J.R.; Argent, S.P.; Ward, M.D. Structural Analysis of Coordination Cage/Guest Complexes Prepared with the 'Crystalline Sponge' Methodology. *Crystals* **2024**, *14*, 873. https://doi.org/10.3390/cryst14100873

Academic Editor: Paola Paoli

Received: 19 September 2024
Revised: 30 September 2024
Accepted: 1 October 2024
Published: 2 October 2024

1. Introduction

In 2013 and 2016, Fujita and co-workers reported, in two seminal papers, the use of porous coordination complexes as hosts for organic guests that could be absorbed into the voids in pre-formed single crystals of the hosts, orienting in the voids in a regular way, allowing single-crystal X-ray crystallography to provide structural characterisation of the bound guests [1,2]. Particular benefits of this 'crystalline sponge' methodology as a tool for structural characterisation of bound guests are that (i) it allows structural analysis by crystallography of molecules that are not themselves crystalline and (ii) it can be performed with microscopic amounts of material (microgram to nanogram scale). Since those original reports from the Fujita group, the technique has been exploited by many other groups and is now an established part of the landscape for structural analysis in supramolecular chemistry [3–12].

As part of our ongoing work on the host/guest chemistry and supramolecular catalysis properties of coordination cages [13,14], particularly using the octanuclear cubic M_8L_{12} cage shown in Figure 1, which is based on an array of 12 ditopic bis(pyrazolyl-pyridine) bridging ligands lying along the edges of an approximate cube of Co(II) ions, we have found the crystalline sponge method to be exceptionally helpful. Coordination cages have attracted immense attention in recent years due to the possibility of functional behaviour associated with their ability to bind guests in the central cavity, with many impressive examples of catalysis in particular being reported [15–30]. We have found that recrystallisation of a coordination cage from a solvent in the presence of any of a wide range of guests afforded crystals of the cage/guest complex only very rarely; nearly always, crystals with an empty cage structure are formed. However, pre-preparation of single crystals of our octanuclear

M_8L_{12} cubic coordination cage (Figure 1) using a solvothermal method [31], followed by immersing a crystal in the guest as either a pure oil or a concentrated methanolic solution for a few hours, resulted in the guest being taken up to the cage cavity—and crystallinity being retained—with a high chance of success. We estimate from many successful and unsuccessful experiments over many years that this method affords around a one in three chance of being able to obtain a crystal structure of a cage/guest complex. Access to synchrotron facilities that provide complete X-ray diffraction datasets in ca. 20 min, coupled with an automatic sample-changing robot that can be operated remotely, has allowed large numbers of successful cage/guest structure determinations to be obtained from each synchrotron session [32].

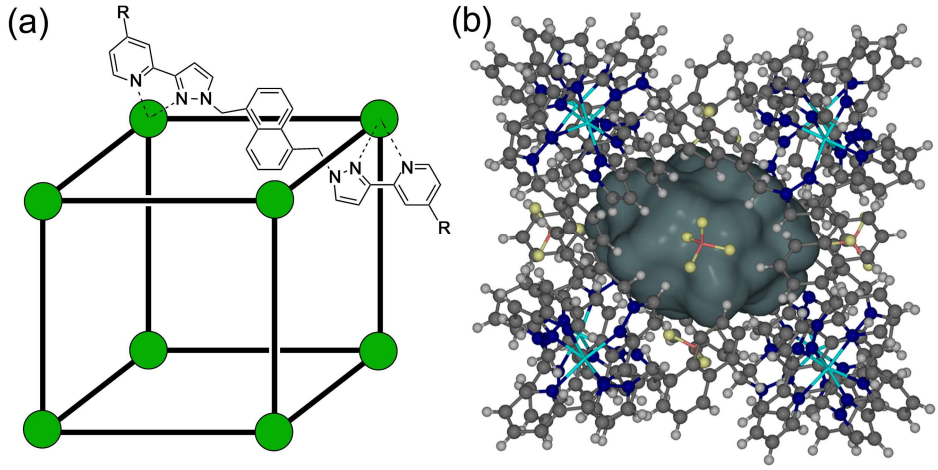

Figure 1. (**a**) Cartoon illustrating the cubic host cage $[M_8L_{12}]^{16+}$, abbreviated as **H** (R = H), emphasising the cubic array of Co(II) ions and the disposition of one bridging ligand. (**b**) A view of the complete cage structure, highlighting the guest-binding cavity space (V = 409 Å^3).

Our motivation is somewhat different from that of Fujita's initial work in that we use relatively small guests, with a focus not on the characterisation of the guest (which is usually structurally simple) but on how the guests interact with the host M_8L_{12} cage. Our interest in this stems from the observation of catalysis in solution afforded by these cages [13,14], which relies on the binding of two different types of guest by quite distinct interactions. Firstly, the cage cavity is hydrophobic and, in aqueous solution, is capable of binding small neutral organic molecules with binding constants of up to $\approx 10^6$ M^{-1} via the hydrophobic effect. The strongest guest binding in solution occurs with guests whose volume is around half of the cavity volume (409 Å^3) [33], in agreement with the Rebek '55% rule' which states, on the basis of empirical studies of thermodynamic stability of a series of host/guest complexes, that the most stable adducts form when the guest volume is in the range 55 ± 9% of the cavity volume [34,35]. Whilst the main thermodynamic binding force underpinning guest binding in water is the hydrophobic effect [33,36], the orientation of cavity-bound guests inside the cavity depends on specific hydrogen-bonding interactions between electron-rich regions of the guest and the cage interior surface [37]; the geometry of this interaction can significantly affect catalytic activity [14].

Secondly, the windows in the centres of the cage faces contain a convergent array of CH protons around their rim, which collectively form an H-bond donor site. Crystal structures of many different salts of the M_8L_{12} cage cation, which carries a 16+ charge, show that the anions X$^-$ invariably bind in the windows around the cage surface, forming multiple charge-assisted CH•••X interactions with the proton array [13]. In aqueous solution, it is clear that these interactions are retained, with hydrophobic and easily-desolvated anions accumulating at these sites around the cage surface [38].

The catalysis that we have observed relies on the interaction of cavity-bound guests with the surface-bound anions, which surround the cavity and thereby afford a high local

concentration of anions around the central guest. The best example is a >10^5-fold rate enhancement of the reaction of cavity-bound benzisoxazole with the surface-bound hydroxides. At a bulk pH of ≈8 in the reaction solution, the accumulation of hydroxide ions around the cage surface is such that the central guest experiences a *local* pH of >13—hence, the observed rate enhancement [39]. Several other catalysed reactions of cage-bound substrates with the local accumulation of anions around the cage surface have been reported [13,14]. It is of particular interest, therefore, to understand the localisation and binding geometries of both neutral guests (usually in the cavity, but sometimes in contact with the exterior surface) and anionic guests (usually at the surface portals). Interactions between both guest types and the cage interior or exterior surface, which help to orient the components with respect to each other during any catalysis, are of particular interest, as is the ability of the cage to bind multiple guests in some cases [32].

As part of this work, we report here the results of an extensive crystallographic investigation into cage/guest complexes based on our M_8L_{12} cage with a wide variety of neutral, cavity-binding guest species. Importantly, whilst solid-state structures are not necessarily wholly representative of solution structures, they still have value in illustrating solution host/guest behaviour given that the cage complex molecules (and their central cavities) remain intact in solution. Thus, crystallographic studies of this nature are useful for informing solution studies on cage/guest catalysis.

2. Materials and Methods

The guests used are shown in Scheme 1. Crystals of the host cage **H** were prepared via a solvothermal method as described previously [31]. In most cases (with guests 1–9), the Co(II) cage was used as the host; for guest 10, the isostructural Zn(II) cage was used. Cage/guest complexes were prepared by prolonged (overnight) immersion of single crystals of **H** in concentrated solutions of the relevant guests in MeOH, as described previously [32]. The crystallographic data were acquired using synchrotron radiation at Beamline I-19, Diamond Light Source, UK [40], using the automatic sample-changing robot [41]; software and methods used for data processing and structure solution and refinement were as reported previously [32]. Detailed information on the crystal properties, data collection, and refinement parameters associated with the structure determinations is compiled in Table 1. Molecular volumes used to determine cavity occupancies were calculated using the 'Molinspiration' software [42]; key parameters associated with guest binding are summarised in Table 2.

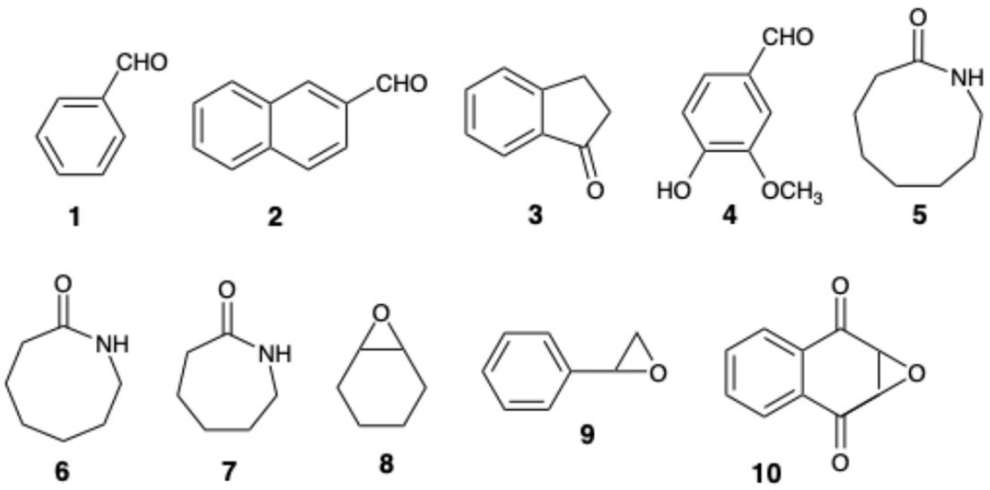

Scheme 1. The set of guests used in this study.

Table 1. Summary of crystallographic, data collection, and refinement parameters for the ten crystal structures in this paper. Items in common to all structures: crystal system and space group are monoclinic, *C*2/c, with $Z = 4$ formula units per unit cell; temperature for data collection = 100(1) K; X-ray wavelength for data collection using the synchrotron source is 0.6889 Å.

Guest	**1**	**2**
Empirical formula	$C_{393}H_{404}B_{16}Co_8F_{64}N_{72}O_{33}$	$C_{382.3}H_{402.4}B_{15}ClCo_8F_{60}N_{72}O_{33.3}$
Formula weight	8524.26	8347.58
Crystal size/mm^3	0.05 × 0.04 × 0.03	0.05 × 0.04 × 0.04
a/Å	33.0615(7)	33.01890(18)
b/Å	29.8386(6)	30.20670(17)
c/Å	40.6176(10)	40.0588(3)
β/degrees	96.149(2)	95.8900(5)
V/Å^3	39,839.0(16)	39,743.4(4)
ρ_{calc}/g cm^{-3}	1.421	1.395
μ/mm^{-1}	0.397	0.402
Reflections collected	256,642	337,342
Data/restraints/parameters	37,813/6507/2507	63,185/6310/2460
Final R indexes [$I \geq 2\sigma(I)$]	$R_1 = 0.0767$, w$R_2 = 0.2222$	$R_1 = 0.0834$, w$R_2 = 0.2665$
Final R indexes (all data)	$R_1 = 0.1008$, w$R_2 = 0.2401$	$R_1 = 0.1251$, w$R_2 = 0.2908$
CCDC number	2384590	2384591
3	**4**	**5**
$C_{384.5}H_{402}B_{15}ClCo_8F_{60}N_{72}O_{32.5}$	$C_{392.96}H_{413.96}B_{16}Co_8F_{64}N_{72}O_{40.73}$	$C_{346.7}H_{289.8}B_{13.8}Cl_{0.6}Co_8F_{55.2}N_{73}O_{3.7}$
8360.80	8657.50	7228.59
0.11 × 0.10 × 0.06	0.12 × 0.10 × 0.09	0.13 × 0.12 × 0.09
32.90637(11)	33.2126(7)	32.92440(7)
29.93692(10)	29.5454(5)	30.18020(6)
40.10059(15)	41.0423(8)	39.98850(8)
96.1742(3)	96.8689(19)	96.4020(2)
39,274.56(17)	39,984.9(13)	39,487.39(14)
1.414	1.438	1.216
0.406	0.398	0.386
24,6676	259,568	343,098
37,249/6271/2442	39,381/6104/2511	62,799/6098/2486
$R_1 = 0.0568$, w$R_2 = 0.1783$	$R_1 = 0.0919$, w$R_2 = 0.3118$	$R_1 = 0.0719$, w$R_2 = 0.2402$
$R_1 = 0.0671$, w$R_2 = 0.1848$	$R_1 = 0.1025$, w$R_2 = 0.3222$	$R_1 = 0.0890$, w$R_2 = 0.2545$
2384592	2384593	2384594
6	**7**	**8**
$C_{345}H_{277}B_{12.4}Co_8F_{49.6}N_{73}O_3$	$C_{377.60}H_{396.80}B_{12.07}Co_8F_{74.9}N_{74.6}O_{2.29}$	$C_{372.32}H_{385.2}B_{16}ClCo_8F_{64}N_{72}O_{27.72}$
7041.26	7963.59	8172.46
0.10 × 0.10 × 0.09	0.04 × 0.04 × 0.06	0.08 × 0.04 × 0.04
32.8556(5)	33.3743(5)	32.8604(3)
29.7412(4)	29.4366(4)	30.0660(2)
39.6625(6)	40.3379(5)	39.7043(6)
96.3677(15)	97.5930(10)	95.4891(11)
38,517.7(10)	39,281.5(9)	39,047.3(6)
1.214	1.347	1.390
0.388	0.393	0.405
28,9312	242,725	285,955

Table 1. *Cont.*

Guest	1	2
47,729/5955/2418	35,993/962/2424	48,386/5809/2293
R_1 = 0.0645, wR_2 = 0.1961	R_1 = 0.1229, wR_2 = 0.3731	R_1 = 0.0796, wR_2 = 0.2630
R_1 = 0.0777, wR_2 = 0.2063	R_1 = 0.1347, wR_2 = 0.3823	R_1 = 0.1230, wR_2 = 0.2868
2384595	2384596	2384627
9	**10**	
$C_{392}H_{368}B_{16}Co_8F_{64}N_{72}O_{21}$	$C_{384.2}H_{412.6}B_{11.6}F_{45.8}N_{72}O_{39.1}$ Zn_8	
8283.96	8182.01	
0.15 × 0.10 × 0.10	0.10 × 0.09 × 0.08	
33.03732(15)	32.8304(3)	
30.04674(14)	29.9021(2)	
40.5695(2)	40.3091(3)	
95.6880(5)	95.8320(10)	
40,073.6(3)	39,366.5(5)	
1.373	1.381	
0.391	0.533	
322,531	537,984	
56,126/8982/2650	50,826/968/2393	
R_1 = 0.0825, wR_2 = 0.2664	R_1 = 0.0743, wR_2 = 0.2413	
R_1 = 0.1189, wR_2 = 0.2966	R_1 = 0.1017, wR_2 = 0.2579	
2384628	2384629	

Table 2. Summary of key features relating to guest binding in the crystal structures.

Guest	Guest Volume/Å^3	Cavity Occupancy	Shortest Co•••O/Å	CH•••O/Å (Naphthyl)	CH•••O/Å (Methylene)
1	103	2 (stacked pair related by inversion, π-π = 3.36 Å)	5.44	2.52–2.70	2.76–2.85
2	147	1.3 (stacked pair related by inversion but with s.o.f. 0.65 each, π-π = 3.44 Å)	5.40	2.42–2.78	2.72–2.83
3	126	2 (stacked pair related by inversion, π-π = 3.49 Å)	5.65	2.53–2.83	2.90–3.05
4	137	2 (stacked pair related by inversion, π-π = 3.30 Å)	5.36	2.54–2.89	2.67–3.00
5	151	1 guest 5 plus two MeOH (0.7/1.0 s.o.f. = 1.7 MeOH), all disordered across cavity inversion centre	5.26	2.50–2.68	2.60–2.64
6	134	1 guest 6 plus two MeOH (both s.o.f. = 0.5), all disordered across cavity inversion centre	5.40	2.47–2.63	2.75–2.79
7	117	1.6 guests 7 (pair related by inversion disordered over two orientations with s.o.f. = 0.4 in each)	5.41/5.56 [a]	2.55–2.83 [a]	2.75–2.94 [a]
8	101	1.72 (pair related by inversion but with site occupancy of 0.86 each)	5.71	2.50–2.56	2.83
9	116	2 (pair related by inversion)	5.35 [b]	2.43–2.88 [b]	2.64–3.00 [b]
10	143	1.3 (pair related by inversion but with site occupancy of 0.65)	5.61	2.53–2.94	2.83–2.98

[a] Two guest orientations disordered both with s.o.f. = 0.4. [b] Based on O(19G) (major disorder component only).

All crystal structure determinations suffered from the usual weak scattering characteristic of crystals of this type, associated with large unit cells and disorder of solvents/anions. This necessitated extensive use of geometric and displacement parameter restraints during the refinements to achieve stable and chemically reasonable models. Some anions/solvents were refined with fractional occupancies over multiple sites when the disorder could be modelled. Large solvent-accessible voids with a diffuse electron density that could not be satisfactorily modelled were accounted for using a solvent mask function during the final refinement. Full details of the treatments of these structures, including the software

used, are given in the individual CIFs. Despite these normal issues associated with anion/solvent disorder, the host cages and their bound guests are generally well behaved, and over-interpretation of minutiae of metric parameters has been avoided.

3. Results and Discussion

The host M_8L_{12} cage that we have studied extensively [13,14] is shown in Figure 1 and contains an approximate cubic array of Co(II) ions with a ditopic bis(pyrazolyl-pyridine) ligand spanning each of the twelve edges; significant intertwining of ligands results in an extensive array of inter-ligand pi-stacking interactions around the exterior surface [31]. The formal molecular symmetry is S_6 as the cage contains two *fac* tris-chelate vertices (at either end of a long diagonal) and six *mer* tris-chelate vertices; as such, it is achiral with an inversion centre. The portals in the six faces of the cage allow ingress and egress of guests—sometimes in fast exchange on the NMR timescale and sometimes in slow exchange, according to guest size and rigidity [13]. Importantly, the two *fac* tris-chelate vertices result in convergent arrays of inwardly directed CH protons from both naphthyl and CH_2 groups which define H-bonding pockets on the interior surface of the cage in regions of high positive electrostatic potential, spatially close to the Co(II) ions; these are the sites where guests containing atoms with lone pairs invariably dock [37].

All crystalline sponge experiments were performed using single crystals of $[M_8L_{12}](BF_4)_{16}$ (M = Co or Zn), which we denote '**H**', for 'host', which were prepared using a solvothermal method reported earlier [31]; in every case, a single crystal was immersed in guest either as a pure oil or as a concentrated MeOH solution overnight before storing under liquid N_2 for X-ray analysis at the Diamond synchrotron facility.

3.1. Aromatic Carbonyl Compounds: Ketones and Aldehydes

The complex of **H** with benzaldehyde (**1**) reveals a stacked pair of guest molecules in the cavity either side of the inversion centre (Figure 2a). The inversion centre necessarily means that the two guests are parallel to one another, with the separation between overlapping aromatic rings being 3.36 Å, a typical graphitic stacking distance. Each guest is disordered over two similar orientations with site occupancies of 0.65/0.35, giving full 100% site occupancy in total for each of the two guests: only the major component is shown in Figure 1 and discussed in detail. The oxygen atom of the guest is directed into the H-bond donor pocket defined by the convergent network of CH groups from the naphthyl C^4 and methylene carbon atoms; it lies 5.44 Å from the nearby Co(II) centre.

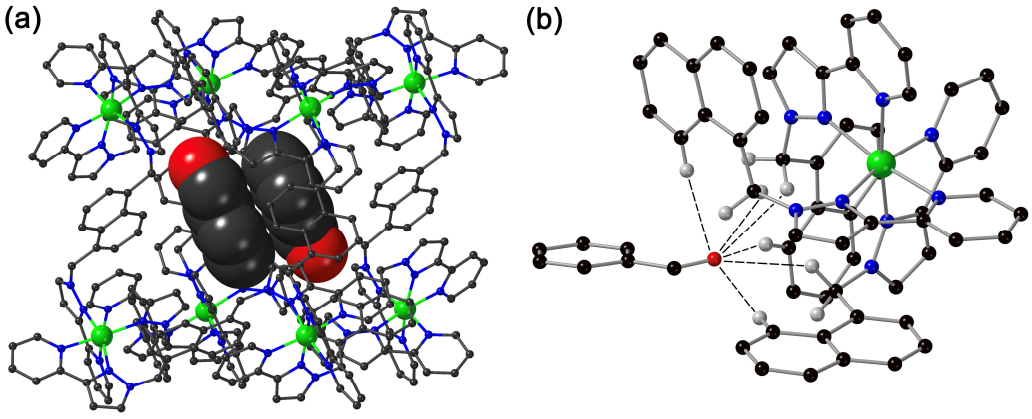

Figure 2. Structure of the complex of **H** with guest **1**. (**a**) A view of the whole cage with the stacked pair of guests shown space-filling; (**b**) a view of one guest and its CH•••O hydrogen-bonding interactions with a *fac* tris-chelate vertex, with H•••O contacts of <3 Å shown by dashed lines.

This projection of the C=O bond into the H-bond donor pocket results in a set of six CH•••O hydrogen-bonding interactions (Figure 2b) with C•••O separations in the range 3.37–3.64 Å and the associated H•••O contacts in the range 2.52–2.70 Å (to naphthyl

CH protons) and 2.76–2.85 Å (to methylene protons). Another benzaldehyde molecule is located outside the cavity in the space between cages, again disordered over two closely spaced positions; this is not discussed further.

This arrangement of a stacked pair of basically planar guests across an inversion centre in the cavity [20], anchored by CH●●●O hydrogen-bonding interactions to the pockets on the cage interior surface, is also observed with the guests 2-napthaldehyde (**2**), 1-indanone (**3**), and 4-hydroxy-3-methoxybenzaldehyde (vanillin, **4**) (Figures 3–5, respectively); the relevant metric data (H-bonding and π-stacking distances, etc.) are collected in Table 2.

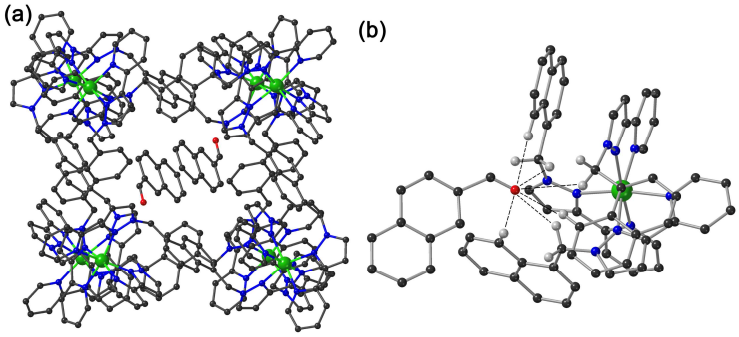

Figure 3. Structure of the complex of **H** with guest **2**. (**a**) A view of the whole cage and the stacked pair of guests; (**b**) a view of one guest and its CH●●●O hydrogen-bonding interactions with a *fac* tris-chelate vertex, with H●●●O contacts of <3 Å shown by dashed lines.

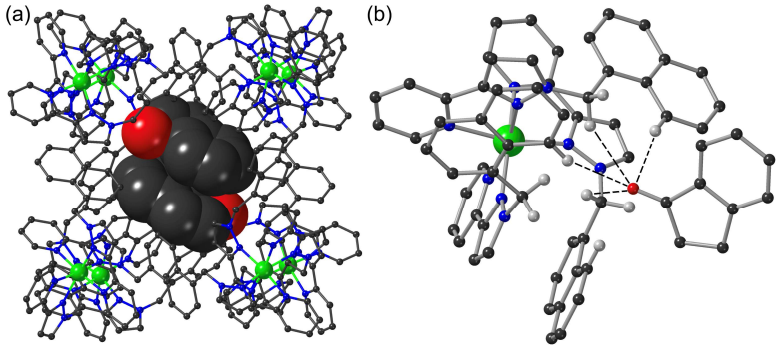

Figure 4. Structure of the complex of **H** with guest **3**. (**a**) A view of the whole cage with the stacked pair of guests shown space-filling; (**b**) a view of one guest and its CH●●●O hydrogen-bonding interactions with a *fac* tris-chelate vertex, with H●●●O contacts of <3 Å shown by dashed lines.

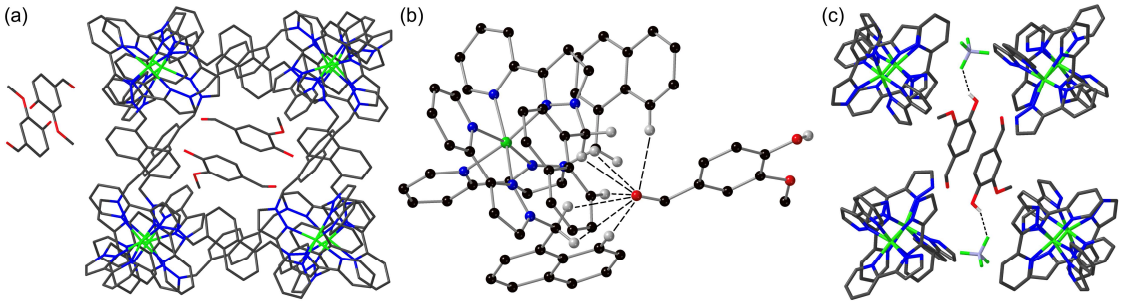

Figure 5. Structure of the complex of **H** with guest **4**. (**a**) A wireframe view of the whole cage with the stacked pair of guests, also showing a stacked pair of guests lying outside the cavity; (**b**) a view of one guest and its CH●●●O hydrogen-bonding interactions with a *fac* tris-chelate vertex, with H●●●O contacts of <3 Å shown by dashed lines; (**c**) a partial wireframe view of the cage (with all naphthyl groups removed for clarity) showing how the stacked pair of cavity-bound guests forms OH●●●F H-bonding interactions with surface-bound fluoroborate anions.

Guest **2** (2-naphthaldehyde, Figure 3) has a site occupancy of 0.65 in each asymmetric unit, leading to an average cavity occupancy of 1.3 guests. Site occupancies of <1 are a common consequence of crystalline sponge experiments because of the time taken for the guest to diffuse to the centre of a crystal, which means that peripheral sites are more likely to be occupied.

Guest **4** (vanillin) contains three oxygen atoms of which it is the aldehyde C=O that 'docks' into the H-bond donor site around the *fac* tris-chelate metal complex vertex (Figure 5); the methoxy group O atom is involved in additional CH●●●O interactions with a naphthyl (C62D) and pyrazolyl (C23B) H atoms with O●●●H distances and 2.85 and 2.69 Å, respectively. This complex contains, in addition to the cavity-bound stacked pair of guests, an additional stacked pair of molecules of **4** across an inversion centre outside the cavity (mean plane separation 3.50 Å; site occupancy 0.62 for each molecule of **4**).

A particularly notable feature of the complex with **4** is that the phenolic proton is not involved in H-bonding to the cage interior surface, but interacts with a fluoroborate ion lying in an adjacent face window, forming an OH●●●F hydrogen bond [the H(17G)●●●F(16) separation—see Figure 5c—is 2.07 Å; the associated O●●●F separation is 2.85 Å]. This ability of surface-bound anions to 'reach into' the cage and interact with cavity-bound guests is precisely the basis of the catalysis in aqueous solution that we have seen in some cases [13,14], with a cage-catalysed Kemp elimination reaction occurring because a surface-bound hydroxide ion can remove a reactive proton from the cavity-bound substrate [39]. This OH●●●F hydrogen bond that we see here is accordingly a nice illustration of what is occurring during solution-phase catalysis.

The presence of a guest pair in the cavity in each of the above cases gives packing coefficients ranging from 50% (benzaldehyde, **1**) to 72% (2-naphthaldehyde, **2**). Whilst the upper limit here is higher than might be expected in solution based on the Rebek 55% principle [34,35], it is not exceptional in the solid state, particularly when an attractive π-π interaction between the guests makes the pair particularly compact; guest packing coefficients approaching 90% have been seen in some cases in the solid state [3,32].

3.2. Aliphatic Lactams

A group of guests that we studied previously as part of a quantitative analysis of the hydrophobic effect is the set of C_8, C_7, and C_6 aliphatic lactams **5**–**7**. In these cases, we could evaluate the incremental contributions of one additional CH_2 group (between **5** and **6**, and between **6** and **7**) on the ΔH and ΔS contributions to guest binding in water [36]. They are of additional interest because of the possibility of catalysed amide hydrolysis associated with accumulation of a high local concentration of hydroxide ions around the bound guests.

The structure of **H** with guest **5** (2-aza-cyclononanone) contains one complete molecule of **5** lying on one side of the cavity, and a pair of MeOH molecules with site occupancies of 0.7 and 1.0 on the other side, i.e., the formulation is **H●5●**$(MeOH)_{1.7}$ (Figure 6). The guests (**5** and the methanol pair) are all disordered across the central inversion centre such that each asymmetric unit apparently contains a molecule of **5** with 0.5 site occupancy superimposed on two MeOH molecules (site occupancies 0.35 and 0.5). If the molecule of **5** and both MeOH molecules are present together, the cavity occupancy is 55%—the centre of the ideal range suggested by Rebek [34,35]. The separation between the O atoms of the two methanol molecules, O(11S)●●●O(15S), is 2.84 Å, which is strongly indicative of an OH●●●O hydrogen bond between the two molecules.

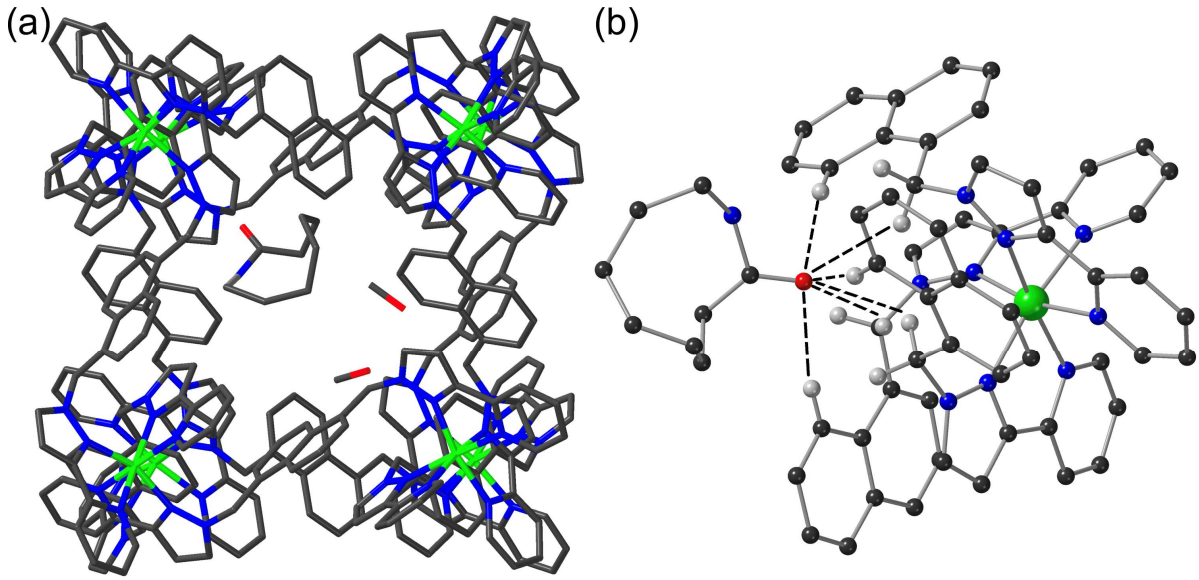

Figure 6. Structure of the complex of **H** with guest **5**. (**a**) A wireframe view of the whole cage with the single guest (plus two MeOH molecules; see Table 2 for details); (**b**) a view of one guest and its CH•••O hydrogen-bonding interactions with a *fac* tris-chelate vertex, with H•••O contacts of <3 Å shown by dashed lines.

Protrusion of the amide O atom into the H-bond donor pocket at one of the *fac* tris-chelate vertices follows the usual pattern with multiple CH•••O contacts with naphthyl and methylene CH protons in the range 2.5–2.7 Å. We also note that the amide N–H proton is directed towards a portal in one of the faces where a $[BF_4]^-$ anion sits, bringing it close to an F atom and forming an NH•••F hydrogen bond, as we saw above with guest **4**. The $[BF_4]^-$ anion is disordered over two closely spaced positions; the shortest NH•••F contact involving the pair of anion sites is 2.38 Å. Clearer examples of similar behaviour are shown in the additional examples with lactam guests **6** and **7**, below.

Removal of one CH_2 group from the guest by using **6** as the guest gives a very similar structure with one molecule of **6** and two of MeOH in the cavity (Figure 7), with the whole set disordered across the inversion centre in the same way as we saw in the previous example **H•5•**$(MeOH)_{1.7}$.

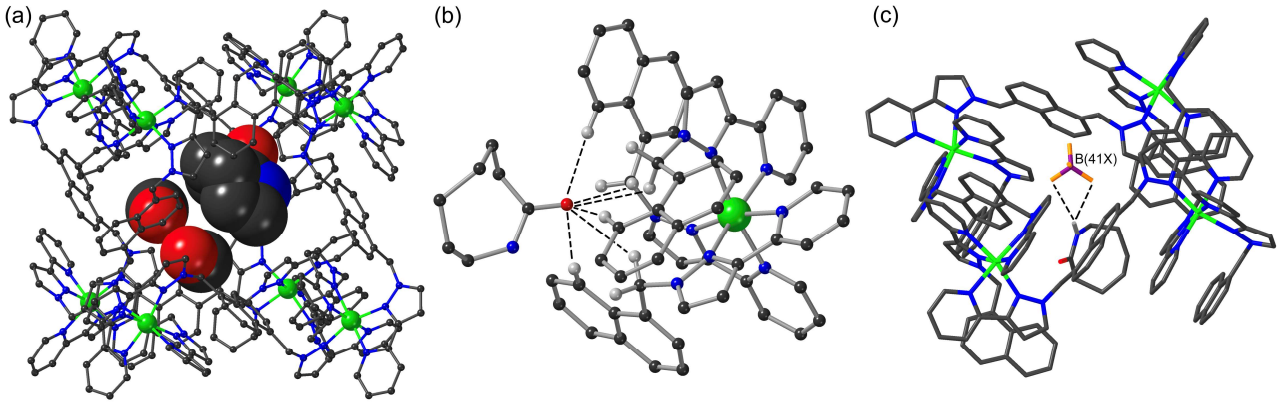

Figure 7. Structure of the complex of **H** with guest **6**. (**a**) A view of the whole cage with the single guest (plus two MeOH molecules; see Table 2 for details) shown in space-filling mode; (**b**) a view of one guest and its CH•••O hydrogen-bonding interactions with a *fac* tris-chelate vertex, with H•••O contacts of <3 Å shown by dashed lines; (**c**) a view of NH•••F hydrogen bonding between the cavity-bound guest **6** and one of the (disordered) surface-bound fluoroborate anions, with H•••F contacts of 2.44 and 2.54 Å shown as dashed lines.

In this case, the fractional site occupancies give a formulation of **H•6•**$(MeOH)_2$, with again an OH•••O hydrogen bond between the two MeOH molecules (O•••O separation 2.80 Å). Again, we see an NH•••F hydrogen-bonding interaction between the guest and a surface-bound $[BF_4]^-$ anion (the shortest non-bonded N•••F separation is 3.09 Å) though the relevant $[BF_4]^-$ anion is disordered over two sites. Overall, the structure of **H•6•**$(MeOH)_2$ is very similar to that of **H•5•**$(MeOH)_{1.7}$.

The complex of **H** with guest **7** (caprolactam; Figure 8) is different in that we see two crystallographically equivalent guest species either side of the inversion centre, in the same way as we see for the aromatic guests shown in the previous section, but the pair is disordered across two significantly different orientations. This is illustrated in Figure 8: each centrosymmetric guest pair, coloured in yellow and purple—but with the amide N atom coloured blue to aid clarity—refines to a site occupancy of 0.4, which means a total cavity occupancy of 1.6 guests. Although the different guest orientations are substantially different for most atoms, the amide O atom is in almost the same position in the two guest orientations, as this is the atom that is anchored to the cage interior surface via CH•••O hydrogen bonding so has little scope to change its position. The two shortest O•••Co separations, for example, are 5.41 and 5.56 Å, and the network of CH•••O interactions is correspondingly comparable between the two guest orientations with several H•••O contacts in the range 2.5–3 Å. The separation between the two guests within a pair, the absence of any solvent molecules which are apparent in the structures with **5** and **6**, and the guest site occupancies indicate that two guest molecules can bind at the same time, which would give a cavity packing coefficient of 57%. An additional pair of guests **7** lying astride an inversion centre, each with a site occupancy of 0.5, forming a mutually NH•••O=C pairwise H-bonding interaction across an inversion centre, is located outside the cavity in the space between cage complexes.

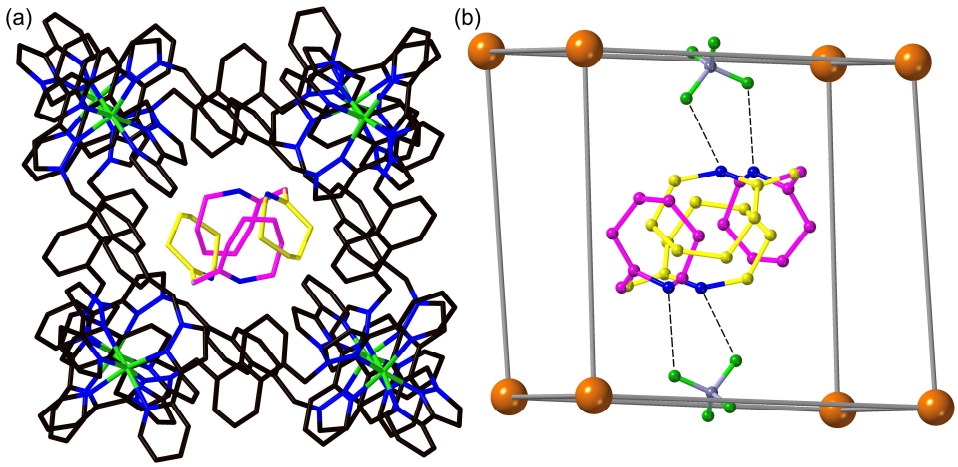

Figure 8. Structure of the complex of **H** with guest **7**. (**a**) A view of the whole cage and the centrosymmetric pair of guests, disordered over two orientations (yellow and purple; N atoms are left blue for clarity). (**b**) A view of the Co_8 polyhedron showing the non-bonded N•••F interactions (all 2.97 Å) which indicate NH•••F hydrogen-bonding interactions of the guests with $(BF_4)^-$ anions in an opposite pair of cage windows.

In addition to the usual network of CH•••O hydrogen bonds (Table 2) arising from the amide O atom projecting into the H-bond donor pocket, we can again see that the NH proton of each guest participates in an NH•••F hydrogen-bonding interaction with a surface-bound BF_4^- anion, with non-bonded N•••F separations (from both guest orientations) of 2.97 Å. These fluoroborate anions that interact with the cavity-bound guests, based on B(5), are refined with a site occupancy of 0.65. For these interactions to occur, the two participating BF_4^- anions (on opposite sides of the cube) need to lie further into the cavity than usual, such that the F atoms F(19) and F(1A) lie within hydrogen-bonding distance

of the NH proton of the cavity-bound guest. We can see this reflected in a particularly short B●●●B separation between the symmetrically equivalent pair of anions on that pair of opposite faces of the cage. The separation between B(5) and its symmetry equivalent across the cube is 10.57 Å, whereas for the other pairs of equivalent anions on opposite sides of the cube, the B●●●B separations are in the range 12–14 Å. Effectively, forming H-bonds to the central guest NH protons has in this case pulled the relevant pair of anions based on B(5) closer in towards the guests in the centre of the cube cavity. As with the structure with guest **4** which displayed similar guest/anion interactions, this can be regarded as a simple illustration of how surface-bound anions interact with cavity-bound guests during the cage-based catalytic processes that we have observed [13,14]. We note that in this structure, the substantial disorder of both guests and fluoroborate anions gives a significantly higher *R*1 value (12.2%) than for the other nine structures (*R*1 in the range 6–9%) and accordingly structural minutiae should not be over-interpreted. However, the basic picture of (a) a centrosymmetric pair of guests disordered over two orientations in the cavity, which (b) is involved in NH●●●F interactions with surface-bound anions, is clear.

3.3. Epoxides

Epoxides are interesting possible guests given their well-known reactivity with anions, which suggests that catalysed reactions of epoxides with anions might be catalysed by the cubic cage if the epoxides can bind in the cage cavity. Three such examples of cage/guest complexes, with cyclohexane epoxide (**8**), styrene epoxide (**9**), and 1,4-naphthoquinone 2,3-epoxide (**10**) as guests, are presented here. In all cases, the guests are compact enough for there to be a pair of them astride the inversion centre, with (as seen in all previous examples) an O atom acting as the H-bond acceptor and projecting into the H-bond donor picket defined by the *fac* tris-chelate H-bond donor pockets.

With guest **8** (Figure 9), the two guests each have a crystallographic site occupancy of 0.86 such that there are 1.72 guests, on average, per cage. With guest **9** (Figure 10), each guest has a total occupancy of 1.0, so there are two per cage, but each is disordered over two sites with fractional occupancies of 0.62 and 0.38, such that the stacked pair has two different orientations. In addition, molecules of **9** were located in the spaces between cages, interacting with the external surfaces, with three such positions having 0.5 site occupancy per asymmetric unit, i.e., three additional complete molecules of **9** per complete cage.

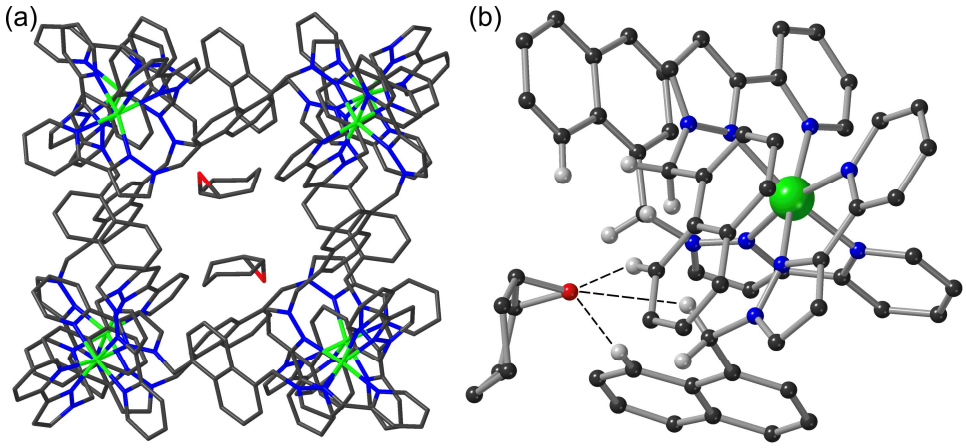

Figure 9. Structure of the complex of **H** with guest **8**. (**a**) A wireframe view of the whole cage and the pair of guests; (**b**) a view of one guest and its CH●●●O hydrogen-bonding interactions with a *fac* tris-chelate vertex, with H●●●O contacts of <3 Å shown by dashed lines.

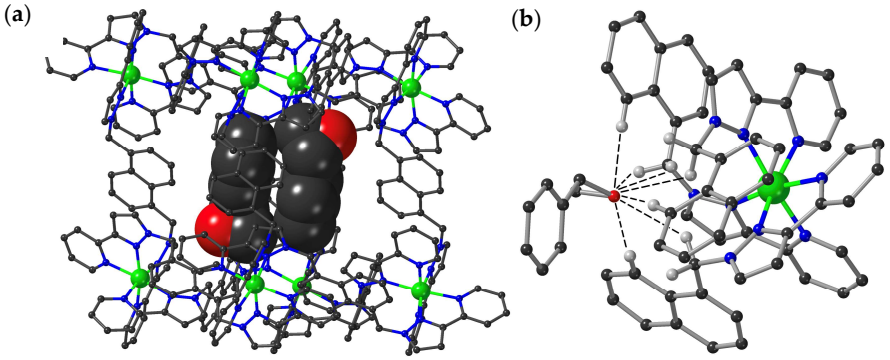

Figure 10. Structure of the complex of **H** with guest **9**. (**a**) A view of the whole cage and the pair of guests shown in space-filling mode (major disorder component only); (**b**) a view of one guest and its CH●●●O hydrogen-bonding interactions with a *fac* tris-chelate vertex, with H●●●O contacts of <3 Å shown by dashed lines (major disorder component only).

These two guests are more compact than all of the others in that the H-bond acceptor group (epoxide O atom) does not protrude from the core of the guest in the same way as it does in all other cases, where a carbonyl C=O group acts as an H-bond acceptor. In order to permit the CH●●●O interactions between the epoxide guests and the H-bond donor pockets on the cage, the guests have to lie close to those binding pockets and hence further apart from each other. Despite the fact that **8** is aliphatic and **9** is aromatic, we see that the distances between the ring units across the inversion centre are similar. The shortest C●●●C contact between the two cyclohexyl rings of **8** is 3.78 Å, which is unremarkable, but the mean separation between the two aromatic rings of guest **9** across the crystallographic inversion centre is an unusually large 3.80 or 3.95 Å (for the two disorder components) in contrast to the more usual 3.3–3.4 Å (*cf.* guests **1**–**4**). This facilitates the CH●●●O interactions of the guests with the cage interior surface; clearly, for guest **9**, these hydrogen-bonding interactions are more significant than any π-π stacking between guests in determining the guest positioning in the cavity.

Guest **10** is significantly bulkier the **8** and **9**: the crystal structure (Figure 11) reveals two in the cage cavity, positioned either side the inversion centre, with site occupancies of 0.65 each (Figure 11). If both are present together, which must be possible sometimes given the site occupancy, the cavity occupancy would be 70%, which is high for a solution-state host/guest complex [34,35] but within normal parameters for solid-state structures [3,32]. In addition, one of the BF_4^- anions based on B(2) protrudes significantly into the cavity in one of its disordered positions and apparently has unfeasibly short contacts with a guest **10**, but the site occupancy of 0.35 for this anion means that this is only present in this position when guest **10** is absent.

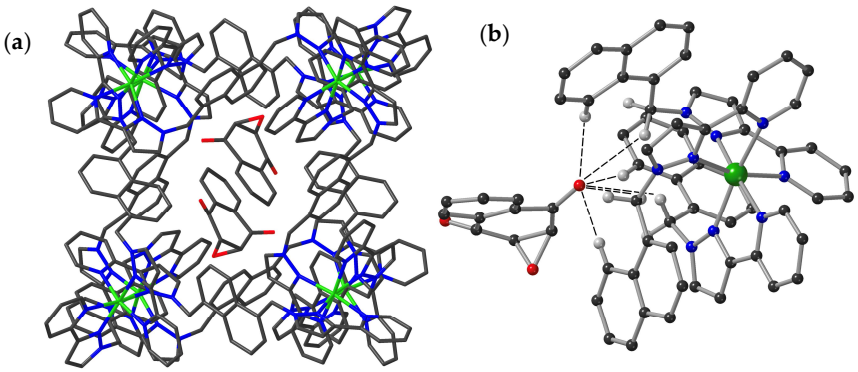

Figure 11. Structure of the complex of **H** with guest **10**. (**a**) A view of the whole cage and the pair of guests shown in wireframe mode; (**b**) a view of one guest and its CH●●●O hydrogen-bonding interactions with a *fac* tris-chelate vertex, with H●●●O contacts of <3 Å shown by dashed lines.

The guest pair of **10** is more tightly packed than we saw with smaller guests **8** and **9**, with a separation of only 3.23 Å between the mean planes of the aromatic rings. However, these do not overlap in a conventional π-stacking manner. The offset between the guests in the centrosymmetric pair means that the aromatic ring of one overlaps principally with the aliphatic ring of the other. It is also interesting to note that, in comparison to the structures with epoxide guests **8** and **9**, in this case, it is one of the carbonyl C=O oxygen atoms rather than the epoxide O atom that is directed into the H-bonding pocket, presumably for simple steric reasons.

4. Conclusions

Crystalline sponge experiments with an octanuclear coordination cage host and a wide range of organic guests have been successful in allowing structural analysis of a range of host/guest complexes in which the guests are taken up into the cage cavity. A common feature of all of these is the hydrogen bonding between the cage interior surface and Lewis basic sites (O atoms, either from C=O bonds in aldehydes, ketones, cyclic amides, or epoxides) which anchors the guests in place. In many cases, small aromatic guests bind as a π-stacked pair; we also see some cyclic aliphatic guests binding in pairs when they are small enough, with the two guests related by inversion in every case. A significant observation in cases where guests (**4**–**7**) contain H-bond donors (a phenol in the case of 4; lactam N-H units for **5**–**7**) is that these can form XH•••F hydrogen-bonding interactions with surface-bound tetrafluoroborate anions, which illustrate nicely the way in which interactions between cavity-bound guests and surface-bound anions promote catalysis in solution. In some cases, guest molecules can also occupy spaces in the lattice outside the cage cavities, interacting with the cage external surface. Overall, such studies inform our understanding of cage/guest binding and thereby provide a valuable complement to solution studies of cage-induced catalysis.

Author Contributions: Conceptualization, project supervision, and manuscript preparation, M.D.W.; sample preparation and crystallographic analysis, C.G.P.T., J.R.W. and S.P.A. All authors have read and agreed to the published version of the manuscript.

Funding: This research was supported in part by EPSRC grant EP/R03382X/1.

Data Availability Statement: The crystallographic data on which this paper is based have been deposited at the Cambridge Crystallographic Data Centre (deposition numbers 2384590–2384595 and 2384627–2384629).

Acknowledgments: We thank the Diamond Light Source for the synchrotron beamtime (proposals CY25064 and CY26668) as well as the staff of beamline I-19—in particular Sarah Barnett—for her expert technical assistance with the data acquisition. Cristina Mozaceanu, Jerico Piper, and Michael Ludden are thanked for their assistance with some of the 'crystalline sponge' sample preparations.

Conflicts of Interest: The authors declare no conflicts of interest. The funders had no role in the design of the study; in the collection, analyses, or interpretation of the data; in the writing of the manuscript; or in the decision to publish the results.

References

1. Inokuma, Y.; Yoshioka, S.; Ariyoshi, J.; Arai, T.; Hitora, Y.; Takada, K.; Matsunaga, S.; Rissanen, K.; Fujita, M. X-ray analysis on the nanogram to microgram scale using porous complexes. *Nature* **2013**, *495*, 461–466. [CrossRef] [PubMed]
2. Hoshino, M.; Khutia, A.; Xing, H.; Inokuma, Y.; Fujita, M. The crystalline sponge method updated. *IUCrJ* **2016**, *3*, 139–151. [CrossRef] [PubMed]
3. Rissanen, K. Crystallography of encapsulated molecules. *Chem. Soc. Rev.* **2017**, *46*, 2638–2648. [CrossRef]
4. Gee, W.J. The growing importance of crystalline molecular flasks and the crystalline sponge method. *Dalton Trans.* **2017**, *46*, 15979–15986. [CrossRef]
5. Du, Q.; Peng, J.; Wu, P.; He, H. Review: Metal-organic framework based crystalline sponge method for structure analysis. *Trends Anal. Chem.* **2018**, *102*, 290–310. [CrossRef]

6. Zigon, N.; Duplan, V.; Wada, N.; Fujita, M. Crystalline sponge method: X-ray structure analysis of small molecules by post-orientation within porous crystals—Principle and proof-of-concept studies. *Angew. Chem. Int. Ed.* **2021**, *60*, 25204–25222. [CrossRef]
7. Habib, F.; Tocher, D.A.; Carmalt, C.J. Applications of the crystalline sponge method and developments of alternative crystalline sponges. *Mater. Today Proc.* **2022**, *56*, 3766–3773. [CrossRef]
8. de Poel, W.; Tinnemans, P.; Duchateau, A.L.L.; Honing, M.; Rutjes, F.P.J.T.; Vlieg, E.; Gelder, R. The crystalline sponge method in water. *Chem. Eur. J.* **2019**, *25*, 14999–15003. [CrossRef]
9. Demakov, P.A.; Ryadun, A.A.; Dybtsev, D.N. Highly luminescent crystalline sponge: Sensing properties and direct X-ray visualisation of the substrates. *Molecules* **2022**, *27*, 8055. [CrossRef]
10. Deng, C.; Song, B.-Q.; Lusi, M.; Bezrukov, A.A.; Haskins, M.M.; Gao, M.-Y.; Peng, Y.-L.; Ma, J.-G.; Cheng, P.; Mukherjee, S.; et al. Crystal engineering of a chiral crystalline sponge that enables absolute structure determination and enantiomeric separation. *Cryst. Growth Des.* **2023**, *23*, 5211–5220. [CrossRef]
11. Yusov, A.; Dillon, A.M.; Chaudhry, M.T.; Newman, J.A.; Lee, A.Y.; Ward, M.D. Benchmarking guanidinium organosulfonate hydrogen-bonded frameworks for structure determination of encapsulated guests. *ACS Mater. Lett.* **2024**, *6*, 1906–1912. [CrossRef] [PubMed]
12. Cardenal, A.D.; Ramadhar, T.R. Application of crystalline matrices for the structural determination or organic molecules. *ACS Cent. Sci.* **2021**, *7*, 406–414. [CrossRef] [PubMed]
13. Ward, M.D.; Hunter, C.A.; Williams, N.H. Coordination cages based on bis(pyrazolylpyridines): Structures, dynamic behaviour, guest binding and catalysis. *Acc. Chem. Res.* **2018**, *51*, 2073–2082. [CrossRef] [PubMed]
14. Ward, M.D. New insights into coordination-cage based catalysis. *Chem. Commun.* **2024**, *60*, 10464–10475. [CrossRef]
15. Brown, C.J.; Toste, F.D.; Bergman, R.G.; Raymond, K.N. Supramolecular catalysis in metal-ligand cluster hosts. *Chem. Rev.* **2015**, *115*, 3012–3035. [CrossRef]
16. Hong, C.M.; Bergman, R.G.; Raymond, K.N.; Toste, F.D. Self-assembled tetrahedral hosts as supramolecular catalysts. *Acc. Chem. Res.* **2018**, *51*, 2447–2455. [CrossRef]
17. Morimoto, M.; Bierschenk, S.M.; Xia, K.T.; Bergman, R.G.; Raymond, K.N.; Toste, F.D. Advances in supramolecular host-mediated reactivity. *Nat. Catal.* **2020**, *3*, 969–984. [CrossRef]
18. Piskorz, T.; Martí-Centelles, V.; Spicer, R.L.; Duarte, F.; Lusby, P.J. Picking the lock of coordination cage catalysis. *Chem. Sci.* **2023**, *14*, 11300–11331. [CrossRef]
19. Jing, X.; He, C.; Zhao, L.; Duan, C. Photochemical properties of host-guest supramolecular systems with structurally confined metal-organic capsules. *Acc. Chem. Res.* **2019**, *52*, 100–109. [CrossRef]
20. Ham, R.; Nielsen, C.J.; Pullen, S.; Reek, J.N.H. Supramolecular coordination cages for artificial photosynthesis and synthetic photocatalysis. *Chem. Rev.* **2023**, *123*, 5225–5261. [CrossRef]
21. Rizzutto, F.J.; von Krbek, L.K.S.; Nitschke, J.R. Strategies for binding multiple guests in metal-organic cages. *Nat. Rev. Chem.* **2019**, *3*, 204–222. [CrossRef]
22. Otte, M. Size-selective molecular flasks. *ACS Catal.* **2016**, *6*, 6491–6510. [CrossRef]
23. Gao, W.-X.; Zhang, H.-N.; Jin, G.-X. Supramolecular catalysis based on discrete heterometallic coordination-driven metallacycles and metallacages. *Coord. Chem. Rev.* **2019**, *386*, 69–84. [CrossRef]
24. Percástegui, E.G.; Ronson, T.K.; Nitschke, J.R. Design and applications of water-soluble coordination cages. *Chem. Rev.* **2020**, *120*, 13480–13544. [CrossRef]
25. DiNardi, R.G.; Rasheed, S.; Capomolla, S.S.; Chak, M.H.; Middleton, I.A.; Macreadie, L.K.; Violi, J.P.; Donald, W.A.; Lusby, P.J.; Beves, J.E. Photoswitchable catalysis by a self-assembled coordination cage. *J. Am. Chem. Soc.* **2024**, *146*, 21196–21202. [CrossRef]
26. Kan, L.; Zhang, L.; Dong, L.-Z.; Wang, X.-H.; Li, R.-H.; Guo, C.; Li, X.; Yan, Y.; Li, S.-L.; Lan, Y.-Q. Bridging the homogeneous and heterogeneous catalysis by supramolecular metal-organic cages with varied packing modes. *Adv. Mater.* **2024**, *36*, 2310061. [CrossRef]
27. Liu, C.-L.; Moussawi, M.A.; Kalandia, G.; Salazar Marcano, D.E.; Shepard, W.E.; Parac-Vogt, T.N. Cavity-directed synthesis of labile polyoxometallates for catalysis in confined spaces. *Angew. Chem. Int. Ed.* **2024**, *63*, e20240190.
28. Ashbridge, Z.; Reek, J.N.H. The multifaceted roles of M_nL_{2n} cages in catalysis. *Nat. Synth.* 2024; *early access*. [CrossRef]
29. Kim, D.; Back, H.J.; An, S.; Han, J.; Jung, O.-S. Selective formation of small and large coordination cages and their catalytic differences. *Inorg. Chem.* **2024**, *63*, 14570–14577. [CrossRef]
30. Hao, Y.; Lu, Y.-L.; Jiao, Z.; Su, C.-Y. Photocatalysis meets confinement: An emerging opportunity for photoinduced organic transformations. *Angew. Chem., Int. Ed.* **2024**, *63*, e202317808. [CrossRef]
31. Tidmarsh, I.S.; Faust, T.B.; Adams, H.; Harding, L.P.; Russo, L.; Clegg, W.; Ward, M.D. Octanuclear cubic coordination cages. *J. Am. Chem. Soc.* **2008**, *130*, 15167–15175. [CrossRef]
32. Taylor, C.G.P.; Argent, A.P.; Ludden, M.D.; Piper, J.P.; Mozaceanu, C.; Barnett, S.A.; Ward, M.D. One guest or two? A crystallographic and solution study of guest binding in a cubic coordination cage. *Chem. Eur. J.* **2020**, *26*, 3054–3064. [CrossRef] [PubMed]
33. Turega, S.; Cullen, W.; Whitehead, M.; Hunter, C.A.; Ward, M.D. Mapping the internal recognition surface of an octanuclear coordination cage using guest libraries. *J. Am. Chem. Soc.* **2014**, *136*, 8475–8483. [CrossRef] [PubMed]

34. Mecozzi, S.; Rebek, J., Jr. The 55% solution: A formula for molecular recognition in the liquid state. *Chem. Eur. J.* **1998**, *4*, 1016–1022. [CrossRef]
35. Rebek, J., Jr. Molecular behaviour in small spaces. *Acc. Chem. Res.* **2009**, *42*, 1660–1668. [CrossRef]
36. Metherell, A.J.; Cullen, W.; Williams, N.H.; Ward, M.D. Binding of hydrophobic guests in a coordination cage cavity is driven by liberation of 'high-energy' water. *Chem. Eur. J.* **2018**, *24*, 1554–1560. [CrossRef]
37. Metherell, A.J.; Ward, M.D. Geometric isomerism in coordination cages based on tris-chelate vertices: A tool to control both assembly and host/guest chemistry. *Dalton Trans.* **2016**, *45*, 16096–16111. [CrossRef]
38. Ludden, M.D.; Ward, M.D. Outside the box: Quantifying interactions of anions with the exterior surface of a cationic coordination cage. *Dalton Trans.* **2021**, *50*, 2782–2791. [CrossRef]
39. Cullen, W.; Misuraca, M.C.; Hunter, C.A.; Williams, N.H.; Ward, M.D. Highly efficient catalysis in the cavity of a cubic coordination cage. *Nat. Chem.* **2016**, *8*, 231–236. [CrossRef]
40. Allan, D.R.; Nowell, H.; Barnett, S.A.; Warren, M.R.; Wilcox, A.; Christensen, J.; Saunders, L.K.; Peach, A.; Hooper, M.T.; Zaja, L.; et al. A novel dual air-bearing fixed-χ diffractometer for small-molecule single-crystal X-ray diffraction on beamline I-19 at Diamond Light Source. *Crystals* **2017**, *7*, 336. [CrossRef]
41. Johnson, N.T.; Waddell, P.G.; Clegg, W.; Probert, M.R. Remote access revolution: Chemical crystallographers enter a new era at Diamond Light Source beamline I-19. *Crystals* **2017**, *7*, 360. [CrossRef]
42. Available online: https://www.molinspiration.com/cgi/properties (accessed on 6 September 2024).